1

2

3

Onset of the aerobic nitrogen cycle during the Great Oxidation Event

5

6

Aubrey L. Zerkle[1*], Simon W. Poulton[2], Robert J. Newton[2], Colin Mettam[1], Mark W. Claire[1,3], Andrey Bekker[4], and Christopher K. Junium[5]

9

[1]*Department of Earth and Environmental Sciences and Centre for Exoplanet Science, University of St Andrews, St Andrews, KY16 9AL, Scotland, UK*

12

[2]*School of Earth & Environment, University of Leeds, Leeds, LS2 9JT, England, UK*

14

[3]*Blue Marble Space Institute of Science, P.O. Box 88561, 98145, Seattle, WA, USA*

16

[4]*Department of Earth Sciences, University of California-Riverside, Riverside, CA, 92521, USA*

19

[5]*Department of Earth Sciences, Syracuse University, Syracuse, NY, 13244, USA*

21

22

23

24

25

28   **The rise of oxygen on early Earth (~2.4 Ga ago)[1] caused a reorganization of**

29   **marine nutrient cycles[2,3], including that of nitrogen, which is important for controlling**

30   **global primary productivity. However, current geochemical records lack the temporal**

31   **resolution to directly address the nature and timing of the biogeochemical response to**

32   **oxygenation[4]. Here we couple records of ocean redox chemistry with nitrogen isotope**

33   **(δ^{15}N) values from ~2.31 billion-year-old shales[5] of the Rooihoogte and Timeball Hill**

34   **formations in South Africa deposited during the early stages of Earth's first rise in**

35   **atmospheric oxygen[6]. Our data fill a ~400 million-year gap in the temporal δ^{15}N record[4]**

36   **and provide evidence for the first pervasive aerobic marine nitrogen cycle. The**

37   **interpretation of our nitrogen isotope data in the context of Fe speciation and carbon**

38   **isotope data suggests biogeochemical cycling across a dynamic redox boundary, with**

39   **primary productivity fuelled by chemoautotrophic production and a nitrogen cycle**

40   **dominated by nitrogen loss processes utilizing newly available marine oxidants. This**

41   **chemostratigraphic trend constrains the onset of widespread nitrate availability**

42   **associated with ocean oxygenation. The rise of marine nitrate could have allowed for the**

43   **rapid diversification and proliferation of nitrate-utilizing cyanobacteria and,**

44   **potentially, eukaryotic phytoplankton.**

45

46

47

48   Nitrogen (N) is an essential element for all living organisms, required alongside

49   carbon (C) and phosphorus (P) for the formation of nucleic acids and proteins. As a result, N

50   and P are the principal limiting nutrients controlling autotrophic CO_2 fixation, which in turn

51   regulates climate, weathering, and the redox state of Earth's surface on geologic timescales.

52   The marine nitrogen cycle is driven largely by biological processes. The primary

53   source of N to the biosphere is nitrogen fixation, the conversion of atmospheric N_2 to organic

54   nitrogen in its bioavailable form (ammonium, NH_4^+). In the modern oceans, ammonium is

55   oxidized via the stepwise process of nitrification, producing nitrite (NO_2^-) and nitrate (NO_3^-).

56   Nitrate (and nitrite) can be assimilated into organic matter, by both oxygenic

57   photoautotrophic bacteria (cyanobacteria) and eukaryotic phytoplankton. Fixed nitrogen is

58   mostly recycled in the water column, but some sinks to the sediments where it is buried

59   and/or remineralized. Some bioavailable nitrogen in the modern oceans is returned to the

60   atmosphere as N_2 via denitrification (the reduction of NO_3^-) and anaerobic ammonium

61   oxidation (anammox, the oxidation of NH_4^+ with NO_2^-) in oxygen-minimum zones[7].

62   Each of these transformations can affect the ratio of nitrogen isotopes ($\delta^{15}N$ =

63    $(^{15}N/^{14}N)_{sample}$ /$(^{15}N/^{14}N)_{atmospheric\ N2}$ − 1, measured in permil, ‰), producing fractionations

64   between reactant and product N species[8]. Nitrogen fixation produces small negative

65   fractionations from atmospheric N_2, resulting in organic $\delta^{15}N$ values of -4 to 0‰[9].

66   Denitrification and anammox preferentially return the lighter isotope to the atmosphere,

67   leaving the residual nitrate and nitrite enriched in ^{15}N by 10-25‰[8,10]. Large fractionations can

68   also be produced by nitrification and biological assimilation[11] (and possibly by dissimilatory

69   nitrate reduction to ammonium[12]). However, these fractionations are not expressed in most

70   modern environments, since nitrification and the recycling of fixed N compounds occur

71   rapidly and nearly quantitatively. Hence, nitrogen loss via denitrification and anammox

72   dominates the modern nitrogen isotope signal, resulting in sedimentary organic matter with

73 average $\delta^{15}N$ values of 7‰[13], due to the uptake of ^{15}N-enriched residual nitrate by primary

74 producers.

75   Beaumont and Robert[2] were the first to suggest a secular trend in the nitrogen isotope

76 values of organic N for Archean and early Proterozoic sediments. They noted that the $\delta^{15}N$ of

77 kerogen in Archean cherts centered at ~0‰ (ranging from -6 to +13‰), while the $\delta^{15}N$ of

78 early Proterozoic kerogens centered at ~5‰, with a total range similar to that in Phanerozoic

79 sediments (~0 to 10‰) (Fig. 1). Our statistical treatment of the temporal $\delta^{15}N$ record

80 (Extended Data Fig. 1) alongside more recent compilations[14] supports this shift, which occurs

81 broadly coeval with the Great Oxidation Event (GOE) from 2.45-2.32 billion-years-ago

82 (Ga)[1,15], although its precise timing remains poorly constrained. As such, the secular rise in

83 $\delta^{15}N$ is commonly interpreted to reflect the transition from an anaerobic nitrogen cycle

84 dominated by reduced N species (N_2 and NH_4^+), to a modern-style aerobic nitrogen cycle

85 with nitrate as a significant component of dissolved inorganic nitrogen. Small (~2 to 5‰)

86 positive excursions in $\delta^{15}N$ within older (~2.6-2.5 Ga) sedimentary rocks have been

87 interpreted to represent the temporary onsets of nitrification/denitrification during transient or

88 localized oxygenation events, which were apparently not sufficiently widespread or long-

89 lived for the signal to persist[16,17]. Alternatively, these small and short-lived positive shifts in

90 $\delta^{15}N$ recorded exclusively in deep-water facies could reflect the incorporation of ^{15}N-enriched

91 NH_4^+ produced by partial nitrification, assimilation of ^{15}N-depleted NH_4^+ in shallow waters,

92 or nitrogen redox cycling independent of surface oxygenation[4,18,19]. To date, however, no

93 records of contemporaneous shallow-water sediments linked directly to records of ocean or

94 atmospheric oxygenation have been available to test these alternatives.

95   Here we examine the response of the nitrogen cycle to changing atmosphere and

96 ocean redox conditions during deposition of ~2.31 Ga siliciclastic rocks, filling a ~400

97 million-year gap in the temporal $\delta^{15}N$ record (Fig. 1), in sediments contemporaneous with the

98   early stages of the GOE. We focus our analyses on the Rooihoogte and Timeball Hill (R-TH)

99   formations, present in drill core EBA-2 in the Potchefstroom Synclinorium, South Africa

100   (Extended Data Fig. 2 and 3). The R-TH form the basal part of the Pretoria Group in the

101   Transvaal basin, and were deposited on a palaeo-delta slope open to the ocean[1]. U-Pb zircon

102   ages for the tuffs in the lower TH give an age of 2.310 ± 0.009 Ga[5]. Atmospheric oxygen

103   content is constrained by the transition from mass-independent to mass-dependent

104   fractionation of sulfur isotopes recently placed within shales of the Rooihoogte Formation[6]

105   (Fig. 2), indicating a rise in atmospheric O_2 levels to greater than 1 ppm[20]. $\delta^{34}S$ data for

106   sedimentary sulfides in the R-TH also indicate a significant rise in seawater sulfate[1,6],

107   consistent with an increase in oxidative weathering of sulfide minerals on the continents.

108   Additional sample information and discussion of post-depositional alteration is available in

109   the Methods and Extended Data Figures 4 and 5.

110   We used a well-established sequential iron extraction technique[21] (the ratio of highly

111   reactive to total Fe, Fe_{HR}/Fe_T, and the ratio of Fe in pyrite to highly reactive Fe, Fe_{Py}/Fe_{HR}) to

112   assess the redox state of the water column during R-TH deposition. Large variations in iron

113   speciation indicate highly dynamic seawater redox conditions during deposition of the

114   Rooihoogte and the lower ~20 m of the TH formations (Fig. 2), with fluctuations between

115   oxic, ferruginous (anoxic and Fe(II)-rich), and euxinic (anoxic and sulfide-rich) states. The

116   rapid changes in water column chemistry suggest that deposition occurred close to a redox

117   interface (chemocline) between oxygenated surface-waters and anoxic deep-waters that were

118   episodically driven euxinic, possibly by variations in organic carbon delivery or seawater

119   sulfate availability. These data also imply the existence of a transiently sulfidic shelf

120   underlying an oxygenated surface ocean, similar to the redox stratification suggested for the

121   Late Archean[22]. Fluctuations in Fe speciation records are accompanied by a significant

122   increase in total organic carbon (from <1 to ~4%) and a decrease in $\delta^{13}C_{org}$ (from -32 to -

123   36‰) across the R-TH boundary (Fig. 2), consistent with chemoautotrophic carbon fixation

124   at or near a chemocline[23].

125   The $\delta^{15}N$ of both bulk nitrogen, $\delta^{15}N_{bulk}$, and extracted kerogen, $\delta^{15}N_{org}$, show a high

126   degree of variability across this same interval (Fig. 2). When interpreted within the context of

127   the Fe speciation data, these values are consistent with a marine nitrogen cycle developed

128   across a dynamic redox boundary. $\delta^{15}N$ values of 6.0 ± 0.5‰ in the lower part of the section

129   are similar to those of modern marine organic matter[13], which reflect a nitrogen cycle

130   dominated by N loss via denitrification and anammox in oxygen minimum zones[24]. Nitrogen

131   isotope values vary from 1.4 to 12‰ across the R-TH boundary, consistent with a variable

132   input from similar chemotrophic communities across a shifting redox interface. These

133   changes could reflect imbalances in ammonium supply and nitrification-denitrification

134   resulting from periodic upwelling of nutrients and high organic productivity. On a stratified

135   Paleoproterozoic marine shelf, uptake of ammonium from anoxic deep waters would have

136   produced ^{15}N-depleted biomass just below the chemocline. Nitrification with newly available

137   marine oxidants would have further enriched residual ammonium in ^{15}N across the redox

138   interface. Higher $\delta^{15}N$ in oxygenated shallow waters could result from the uptake of this ^{15}N-

139   enriched ammonium, or by nitrate assimilation once nitrate levels rose high enough to

140   support partial denitrification. The $\delta^{15}N$ stabilizes at near modern values (7.2 ± 1.0‰) up-

141   section in the lower TH, in association with Fe speciation data indicative of the onset of

142   pervasively oxygenated shallower water conditions. Oxygenation of surface waters would

143   have supported widespread nitrification and further enhanced nitrate availability.

144   Notably, within the context of the global $\delta^{15}N$ record (Fig. 1), the R-TH succession

145   records the first clear evidence for a long-lived aerobic nitrogen cycle in the sedimentary

146   record. The ~2.31 Ga R-TH section, deposited at the heart of the GOE and coincident with

147   the permanent loss of mass independent S isotope fractionation[6], is bracketed by evidence for

148   only transient aerobic nitrogen cycling in older sediments (from ~2.7 to 2.5 Ga[16,17,19]), and

149   the clear isotopic imprint of aerobic nitrogen cycling in records from younger sediments

150   deposited after ~2.0 Ga[25-28], as confirmed by statistical analysis of the global database

151   (Extended Data Fig. 1). Available data suggests that earlier transient oxygenation events were

152   insufficient to establish the modern nitrogen cycle, as marine nitrate was not pervasive in the

153   oceans before the GOE[16,17]. In addition, $\delta^{15}N$ values > 2‰ are typical for the remainder of the

154   Precambrian record (Fig. 1), indicating that aerobic nitrogen cycling became at least locally

155   widespread enough to impart a long-lived isotopic imprint on marine $\delta^{15}N$ during the GOE.

156   The build-up of a significant marine nitrate reservoir would have provided an

157   important evolutionary driver, as prokaryotes and eukaryotic phytoplankton that were able to

158   utilize nitrate as a primary nutrient source could have diversified to fill this new ecological

159   niche. The co-occurrence of this event with other geochemical changes indicative of the first

160   significant oxygenation of Earth's atmosphere provides a crucial constraint on the

161   surprisingly rapid response time of the global biosphere to this major transition in Earth

162   surface chemistry.

163

164   **References**

165   1   Bekker, A. *et al.* Dating the rise of atmospheric oxygen. *Nature* **427**, 117-120 (2004).

166   2   Beaumont, V. & Robert, F. Nitrogen isotope ratios of kerogens in Precambrian cherts:

167   a record of the evolution of atmosphere chemistry? *Precambrian Research* **96**, 63-82

168   (1999).

169   3   Bekker, A. & Holland, H. D. Oxygen overshoot and recovery during the early

170   Paleoproterozoic. *Earth and Planetary Science Letters* **317-318**, 295-304 (2012).

171   4   Stueken, E. E., Kipp, M. A., Koehler, M. C. & Buick, R. The evolution of Earth's

172   biogeochemical nitrogen cycle. *Earth-Science Reviews* **160**, 220-239 (2016).

173   5   Rasmussen, B., Bekker, A. & Fletcher, I. R. Correlations of Paleoproterozoic

174   glaciations based on U-Pb zircon ages for tuff beds in the Transvaal and Huronian

175   Supergroups. *Earth and Planetary Science Letters* **382**, 173-180 (2013).

176   6   Luo, G. *et al.* Rapid oxygenation of Earth's atmosphere 2.33 billion years ago. *Science*

177   *Advances* **2**, 1-9 (2016).

178   7   Dalsgaard, T., Thamdrup, B., Farias, L. & Revsbech, N. P. Anammox and

179   denitrification in the oxygen minimum zone of the eastern South Pacific. *Limnology*

180   *and Oceanography* **57**, 1331-1346 (2012).

181   8   Wada, E. in *Isotope Marine Chemistry* (eds E. D. Goldberg, Y. Horibe, & K.

182   Saruhashi) 375-398 (Uchida Rokakuho, 1980).

183   9   Zerkle, A. L., Junium, C. K., Canfield, D. E. & House, C. H. Production of 15N-

184   depleted biomass during cyanobacterial N2-fixation at high Fe concentrations.

185   *Journal of Geophysical Research* **113** (2008).

186   10 Brunner, B. *et al.* Nitrogen isotope effects induced by anammox bacteria. *Proceedings*

187   *of the National Academy of Sciences* **110**, 18994-18999 (2013).

188   11 Hoch, M. P., Fogel, M. L. & Kirchman, D. L. Isotope fractionation associated with

189   ammonium uptake by a marine bacterium. *Limnology and Oceanography* **37**, 1447-

190   1459 (1992).

191   12 McCready, R. G. L., Gould, W. D. & Barendregt, R. W. Nitrogen isotope

192   fractionation during the reduction of NO3- to NH4+ by Desulfovibrio sp. *Canadian*

193   *Journal of Microbiology* **29**, 231-234 (1983).

194   13 Peters, K. E., Sweeney, R. E. & Kaplan, I. R. Correlation of carbon and nitrogen

195   stable isotope ratios in sedimentary organic matter. *Limnology and Oceanography* **23**,

196   598-604 (1978).

197   14   Ader, M. *et al.* Interpretation of the nitrogen isotopic composition of Precambrian

198   sedimentary rocks: Assumptions and perspectives. *Chemical Geology* **429**, 93-110

199   (2016).

200   15   Farquhar, J., Zerkle, A. L. & Bekker, A. Geological constraints on the origin of

201   oxygenic photosynthesis. *Photosynthesis Research* **107**, 11-36 (2011).

202   16   Garvin, J., Buick, R., Anbar, A. D., Arnold, G. L. & Kaufman, A. J. Isotopic evidence

203   for an aerobic nitrogen cycle in the latest Archean. *Science* **323**, 1045-1048 (2009).

204   17   Godfrey, L. V. & Falkowski, P. G. The cycling and redox state of nitrogen in the

205   Archaean ocean. *Nature Geoscience*, doi:DOI: 10.1038/NGEO633 (2009).

206   18   Thomazo, C., Ader, M. & Philippot, P. Extreme 15N-enrichments in 2.72-Gyr-old

207   sediments: evidence for a turning point in the nitrogen cycle. *Geobiology* **9**, 107-120

208   (2011).

209   19   Busigny, V., Lebeau, O., Ader, M., Krapez, B. & Bekker, A. Nitrogen cycle in the

210   Late Archean ferruginous ocean. *Chemical Geology* **362**, 115-130 (2013).

211   20   Pavlov, A. A. & Kasting, J. F. Mass-independent fractionation of sulfur isotopes in

212   Archean sediments: Strong evidence for an anoxic Archean atmosphere. *Astrobiology*

213   **2**, 27-41 (2002).

214   21   Poulton, S. W. & Canfield, D. E. Development of a sequential extraction procedure

215   for iron: implications for iron partitioning in continentally derived particulates.

216   *Chemical Geology* **214**, 209-221 (2005).

217   22   Reinhard, C. T., Raiswell, R., Scott, C., Anbar, A. D. & Lyons, T. W. A late Archean

218   sulfidic sea stimulated by early oxidative weathering of the continents. *Science* **326**,

219   713-716 (2009).

220   23   Coetzee, L. L., Beukes, N. J., Gutzmer, J. & Kakegawa, T. Links of organic carbon

221   cycling and burial to depositional depth gradients and establishment of a snowball

222   Earth at 2.3Ga. Evidence from the Timeball Hill Formation, Transvaal Supergroup,

223   South Africa. *South African Journal of Geology* **109**, 109-122 (2006).

224 24 De Pol-Holz, R., Robinson, R. S., Hebbeln, D., Sigman, D. M. & Ulloa, O. Controls

225   on sedimentary nitrogen isotopes along the Chile margin. *Deep-Sea Research Part Ii-*

226   *Topical Studies in Oceanography* **56**, 1100-1112, doi:10.1016/j.dsr2.2008.09.014

227   (2009).

228 25 Godfrey, L. V., Poulton, S. W., Bebout, G. E. & Fralick, P. W. Stability of the

229   nitrogen cycle during development of sulfidic water in the redox-stratified late

230   Paleoproterozoic Ocean. *Geology* **41**, 655-658 (2013).

231 26 Stueken, E. E. A test of the nitrogen-limitation hypothesis for retarded eukaryote

232   radiation: Nitrogen isotopes across a Mesoproterozoic basinal profile. *Geochimica et*

233   *Cosmochimica Acta* **120**, 121-139 (2013).

234 27 Papineau, D. *et al.* High primary productivity and nitrogen cycling after the

235   Paleoproterozoic phosphogenic event in the Aravalli Supergroup, India. *Precambrian*

236   *Research* **171**, 37-56, doi:10.1016/j.precamres.2009.03.005 (2009).

237 28 Kump, L. R. *et al.* Isotopic evidence for massive oxidation of organic matter

238   following the Great Oxidation Event. *Science* **334**, 1694-1696 (2011).

239 29 Farquhar, J., Zerkle, A. L. & Bekker, A. in *Treatise in Geochemistry: Reference*

240   *Module in Earth Systems and Environmental Sciences* Vol. 6 (eds H. D. Holland &

241   K. Turekian) 91-138 (Elsevier, 2014).

242

243 Acknowledgements

246   the staff at the National Core Library in Donkerhoek for facilitating access to the core

247   materials, and Misuk Yun for assistance with stable isotope analyses at U. Manitoba.

248

249   **Author contributions**

250   AZ and SP conceived the study; SP and AB collected the samples; AZ, SP, RN, CM,

251   and CJ processed samples and performed geochemical analyses; MC provided statistical

252   analyses of the global database; AZ interpreted the data and wrote the manuscript with input

253   from all coauthors.

254

255   **Declaration of competing interests**

256   The authors declare no competing financial interests.

257

258   **Figure Legends**

259   Figure 1. Secular trend in sedimentary $\delta^{15}N$ over early Earth history, from Farquhar et al.[29],

260   with references listed therein. "Mineral N" refers to nitrogen extracted as ammonium from

261   phyllosilicates. Red and purple data points are from this study, denoting kerogen and bulk

262   rock analyses, respectively.

263

264   Figure 2. Lithological and geochemical data for core EBA-2, illustrating the R-TH overlying

265   the Great Chert Breccia (GCB), which developed at the top of the Malmani carbonate

266   platform. Data include Fe speciation, TOC, and $\delta^{13}C_{org}$ spanning the section. Fe_{Py}/Fe_{HR} data

267   are only shown for samples with Fe_{HR}/Fe_T suggesting anoxic deposition. Inset is a blow-up of

268      $\delta^{15}N$ values, alongside TOC and $\delta^{13}C_{org}$, for the R-TH boundary (red bar). For $\delta^{15}N$, red data

269   points are extracted kerogen, purple data points are bulk rock N, and empty symbols are

270　　nano-EA analyses. For all data, errors are within the size of the symbols. The orange arrows

271　　denote the disappearance of S-MIF in EBA-2[6].

272

273　　**METHODS**

274　　**Statistical analysis of δ^{15}N database**

275　　　　　Previous studies have utilized age-binned means of the δ^{15}N database over hand-

276　　picked geologic intervals to propose changes in this proxy with time[2,4,14,30]. These studies

277　　have provided a qualitative indication that the δ^{15}N record appears to vary systematically over

278　　geologic time; however, they are not statistically robust, because two samples drawn from a

279　　single population will often express different means due to random noise. A Student's T-test

280　　is a more statistically robust method for determining if two (otherwise normally-distributed)

281　　sample sets are likely to arise from the same population, which is considered the null

282　　hypothesis. We therefore performed 754 independent two-tailed T-tests spanning every

283　　possible time-weighted binning of the δ^{15}N database, assuming unequal variances in the

284　　sample sets. In all but a few cases at the extremes (where the bin sizes of one of the sample

285　　sets were small), the null hypothesis was rejected at greater than 99% confidence and so the

286　　divided sample sets are shown to arise from populations with different means and variances.

287　　　　　The sample sets are defined as ranging from the first database entry from the

288　　Proterozoic, at 0.70 Ga, to the entry with the age shown on the horizontal axis of Extended

289　　Data Figure 1, and then from the subsequent entry to our final database entry, with age of

290　　3.80 Ga. Extended Data Figure 1 shows the "false-positive" probability that the two samples

291　　sets arise from populations of the same mean and variance. Using this method, datasets at

292　　2.31 Ga (this study), 2.50 Ga, and 2.70-2.80 Ga are demonstrated to be the most statistically

293　　meaningful pivot-ages which separate the database into distinct samples sets.

294   As discussed in the manuscript, the large number of database entries from ~2.50 Ga

295   stem from predominantly deep water environments which show small stratigraphic shifts in

296     $\delta^{15}N$ interpreted to reflect temporary localized nitrification/denitrification in an otherwise

297   reducing ocean[16,17,19]. As a result, the global database may be slightly biased toward results

298   showing an "oxic" nitrogen cycle at this time period. The data presented in this study are

299   from unequivocally oxic shallow waters, and the statistical analysis confirms that our new

300   data provide a stronger statistical power in separating the data sets, even given the bias in the

301   database at 2.50 Ga. As we note in the main text, additional $\delta^{15}N$ data from shallow water

302   depositional environments in this crucial interval are required to test alternative hypotheses.

303   Although beyond the scope of this current study, we additionally note that the most

304   statistically meaningful separation of the $\delta^{15}N$ database occurs when the sample sets are split

305   between 0.70 – 2.71 Ga and between 2.75– 3.80 Ga. The statistical power for this split is

306   driven primarily by the predominance of extremely ^{15}N-enriched $\delta^{15}N$ measurements

307   (upwards of +55‰, dominantly in kerogens) from this time period. The origin of these

308   extreme values is highly debated, with hypotheses including the onset of partial

309   nitrification[18], and effects from ammonia degassing under highly alkaline conditions[31].

310   Regardless, it is clear the ~2.70 Ga data do not represent a modern-style aerobic N cycle, as

311   no such extreme values are seen anywhere in the modern Earth system. These statistical

312   analyses therefore demonstrate that the nitrogen cycle underwent massive changes in both the

313   early Neoarchean[31] and at the GOE, with the data from this study forming the key pivot point

314   for the latter.

315   **Fe and C analyses**

316   Iron speciation was determined by means of the sequential extraction technique

317   described in Poulton and Canfield[21], with a RSD of <5% for all extraction steps. TOC was

318   measured on a Leco analyzer after decarbonation by treatment with 20% HCl, with a 1σ of

319   0.05%. $\delta^{13}C_{org}$ was measured at the SIFIR Laboratory at the University of Manitoba. A

320   calibration line was calculated by least squares linear regression of analyses of two

321   international standards (USGS40, USGS41) performed at the beginning, middle and end of

322   each run. Replicate analyses of international standard USGS Green River shale SGR-1b

323   ($\delta^{13}C_{org}$ = -29.3±0.1‰ VPDB) alongside unknown samples yielded the results of $\delta^{13}C_{org}$ = -

324   29.5±0.2‰ (n=29).

325   **Kerogen-N isotope analyses**

326   Kerogen was extracted following a method modified from McKirdy and Powell[32] in

327   the Geobiology laboratory at the University of St Andrews. Approximately 100-200 mg of

328   bulk rock powders were decarbonated twice with 10% (v/v) HCl overnight at 40˚C in a clean

329   hood, then transferred to Teflon beakers in a dedicated fume cupboard, where 5mL of 10%

330   HCl + 2mL of concentrated HF was added and volatilized at 40˚C. Residues were rinsed 5x

331   with Milli-Q water. Chloroform was added to the residue, shaken, and allowed to settle in

332   separation funnels for ~30 minutes. Heavy minerals that sank to the bottom were first

333   removed, and then floated kerogen was transferred to a Teflon beaker, dried in a clean hood,

334   and stored in an anaerobic chamber until analysis. A subset of samples were also extracted

335   commercially at Global Geolab Ltd, using techniques similar to those above, except that

336   kerogens were separated out by heavy liquid separation with zinc bromide instead of

337   chloroform. Repeat extracts of the same sample (all plotted in Fig. 2) had consistent $\delta^{15}N_{org}$

338   values between labs, generally within 1‰ (Source Data).

339   Kerogen N isotope ratios ($\delta^{15}N_{org}$) were measured using a Eurovector 3028HT

340   elemental analyser fitted with a Costech Zero Blank autosampler coupled to an Isoprime

341   isotope ratio mass spectrometer, at the University of Leeds. Columns with reagents were

342   fitted to the EA along with either a high-resolution CN GC column (Elemental Microanalysis

343   E3037), or a NCH column (Elemental Microanalysis E3001), as below. A magnesium

344 perchlorate-carbosorb trap was used to trap water and CO_2. The setup was leak checked and

345 then the combustion and reduction furnaces were heated to operating temperatures and left

346 purging with He overnight. The combustion furnace was held at 1020°C and the reduction

347 furnace at 650°C. The GC column was baked at 190°C with He flowing overnight, and then

348 its temperature was reduced to the normal running temperature (80°C for the NCH column,

349 and 110°C for the high resolution CN column).

350   Samples were prepared by weighing between 10 and 30 mg of kerogen into 8 x 5 mm

351 tin cups. These were loaded into the autosampler and purged for at least an hour before

352 analyses. Upon sealing the autosampler chamber and opening it to the main He flow, mass 28

353 was monitored until it returned to a stable background (less than $7e^{-11}$ nA). Samples were

354 combusted in a pulse of pure oxygen (N5.0 grade, BOC, UK) and injected into a stream of

355 helium (CP grade, BOC, UK). The resulting gases were passed through chromous oxide and

356 silvered cobaltous oxide, fine copper wires, and a magnesium pechlorate/carbosorb trap

357 before entering the GC column. The mass 29/28 ratio of the sample N_2 gas was measured

358 relative to a pulse of pure N_2 (Research grade, BOC, UK) and corrected to the AIR scale

359 using the USGS-25 and USGS-26 ammonium sulfate standards, with $\delta^{15}N_{AIR}$ values of -

360 30.1‰ and +53.7‰, respectively. Repeated runs of standard materials during each analytical

361 session produced standard deviations of the raw $\delta^{15}N_{refgas}$ that were generally between 0.15

362 and 0.41‰, with the majority ≤ 0.30‰. Data were corrected with bracketing standards using

363 a simple linear regression equation. Repeats of an in-house yeast standard (7.6 wt% N) gave a

364 long-term average value of -0.8 ±0.31‰ (1σ, 37 runs with both NCH and high-resolution CN

365 GC columns), with in-run reproducibility always ≤ 0.2‰ where 3 or more repeats were

366 measured during the same analytical session. A sample size test using the same yeast

367 standard determined that samples producing peak heights of < 1nA have larger variability,

368 approaching the blank $\delta^{15}N$ value as their peak height decreased. Repeat analyses of the yeast

369   standard with peak height > 1 nA produced $\delta^{15}N_{refgas}$ values that differed by ≤ 0.1‰.

370   Therefore, analyses that produced peak heights of < 1nA were discarded in this study.

371   The analysis of organic materials with low concentrations of nitrogen can be

372   complicated by the production of CO gas (at masses 28 and 29) as a result of incomplete

373   combustion, which can alter the apparent $^{15}N/^{14}N$ ratio of the sample. We took the following

374   precautions to ensure that data were not affected by CO production during incomplete

375   combustion: 1) combustion tests using a low-N organic material (cornflower, 0.07 wt% N);

376   2) mass 30 monitoring; and, 3) use of NCH column to produce a better separation between

377   the N_2 and unwanted CO that might produce a secondary mass 28 peak for samples affected

378   by partial combustion.

379   **Bulk-rock analyses**

380   A subset of R-TH samples was analysed for bulk rock geochemistry (wt % K_2O) to

381   screen for post-depositional alteration at the University of St Andrews, using standard X-ray

382   fluorescence (with 1σ of 0.02 wt%). Bulk nitrogen content (% TN) and bulk $\delta^{15}N$ ($\delta^{15}N_{bulk}$,

383   without decarbonation) were measured at the SIFIR Laboratory at the University of

384   Manitoba. Analyses were performed using a Costech^{TM} 4010 Elemental Analyzer (EA) fitted

385   with a Costech Zero Blank autosampler and coupled to a Thermo Finnigan^{TM} Delta V Plus

386   isotope-ratio mass-spectrometer via an open-split interface (ConFlo III, Thermo Finnigan^{TM}).

387   A magnesium perchlorate-carbosorb trap was placed before the ConFlo III to remove

388   remaining water and CO_2. In order to improve the efficiency of sample combustion,

389   temperature in the oxidation column was raised to 1050°C, and a 'macro' O_2 injection loop

390   was utilized. The setup was leak checked and then the oxidation and reduction columns were

391   heated to operating temperatures and left purging with He overnight. The oxidation column

392   was held at 1050°C and the reduction column at 650°C. The ~3 m-long stainless steel GC

393   column was baked at 100-110°C with He flowing overnight, and then its temperature was

394 reduced to the normal running temperature (55°C). CO_2 level was monitored during

395 analytical sessions. Sample normalization was performed using the two-point calibration

396 described in Coplen et al.[33], by analyzing two international standards (USGS40 and USGS41)

397 at the beginning, middle, and end of each analytical session. Two certified standards were

398 additionally analyzed alongside with samples: B2153, soil, % TN = 0.13 ± 0.02%, $\delta^{15}N_{air}$ =

399 +6.70 ± 0.15‰ (Elemental Microanalysis); and SDO-1, Devonian Ohio Shale, % TN = 0.36

400 ± 0.01%, $\delta^{15}N_{air}$ = -0.8 ± 0.3‰ (USGS). The data obtained were % TN = 0.14 ± 0.00% and

401 $\delta^{15}N_{air}$ values of +6.76 ± 0.02‰ (n=3) for B2153, and % TN = 0.37 ± 0.00% and -0.32 ±

402 0.02‰ (n=3) for SDO-1.

403 **Nano-EA-IRMS analyses**

404 A subset of extracted kerogens and bulk rock powders were also run for $\delta^{15}N$ by

405 nano-EA-IRMS at Syracuse University, following methods outlined in Polissar et al.[34] The

406 benefit of this approach is that it is specifically designed for analysis of as little as 0.5 mg of

407 kerogen and 50 nanomoles of N, thus limiting some of the complications associated with

408 achieving complete combustion on larger samples. Encapsulated sample powders were

409 evacuated to remove atmospheric N_2 present in capsule pore space and purged with Ar.

410 Sample combustion was performed in an Elementar Isotope Cube elemental analyser with

411 reaction conditions set at 1100°C and 650°C for the oxidation and reduction reactors,

412 respectively. Oxygen flow was set a 30 ml*min^{-1} and introduced to the helium stream for 90

413 seconds, initiating when the sample is dropped into the oxidation reactor. The EA is coupled

414 to an automated cryotrapping system that was build using a modified Elementar TraceGas

415 analyser. The generated N_2 gas was trapped in a silica gel-filled, stainless steel trap cooled in

416 liquid N_2. Following complete collection of the N_2 peak from the high-flow EA, the He flow

417 through the cryotrap was switched to a lower flow (2 ml*min^{-1}) via actuation of a VICI Valco

418 6-port valve. The trap was heated and N_2 was released to a room temperature capillary GC-

419   column (JW CarboBOND, 25 m, 0.53 mm ID, 5 μm), and ultimately to the IRMS. The

420   Elementar EA traps CO_2 from combustion in a molecular sieve trap that is released to waste

421   or to the IRMS directly for $\delta^{13}C$ analyses. This ensures that CO_2 is not trapped in the N_2

422   cryotrap and mitigates the potential for neo-formed CO within the ion source. All samples

423   were run in triplicate and blank-corrected using Keeling-style plots and normalized using the

424   2pt-correction scheme detailed in Coplen *et al.*[33] Use of Keeling plots allows for simple

425   estimation of the influence of the N_2 procedural blank on samples and for high fidelity

426   measurements of $\delta^{15}N$ on the small sample sizes employed. Reproducibility of replicates

427   analyses of standards [IAEA N1 (0.4‰) and N2 (+20.35‰) and NIST Peach Leaves

428   (1.98‰)] and samples was ± 0.26‰.

429   **Additional analyses and data fidelity**

430   Nitrogen is preserved in the sedimentary rock record primarily as organic N or as

431   ammonium substituting for potassium in phyllosilicates[35]. The sedimentary N isotope values

432   can be modified by a number of post-depositional processes, including diagenesis, burial, and

433   metamorphism. Therefore, before interpreting sedimentary $\delta^{15}N$ data, it is first necessary to

434   examine the possible impacts of post-depositional alteration on the primary signal. Here we

435   examine trends in supplementary and bulk-rock data in order to validate our $\delta^{15}N$ dataset as

436   representing a primary signal.

437   Degradation of organic matter during early diagenesis can offset primary $\delta^{15}N$ signals

438   by 2 to 3‰[36]. High-pressure metamorphism does not impart significant $\delta^{15}N$ changes [37],

439   although high-temperature metamorphism can increase $\delta^{15}N$ in ammoniated phyllosilicates

440   (and possibly N_{org}; but see Ader *et al.* [38]) due to volatilization of ^{15}N-depleted nitrogen[35,37].

441   Since the R-TH has only experienced lower greenschist facies metamorphism[23], this

442   mechanism would be expected to produce at most a 1-2‰ positive shift in $\delta^{15}N_{org}$. Cross-

443   plots demonstrate no correlation between % N in kerogen (N_{org}) and $\delta^{15}N_{org}$ values (Extended

444   Data Fig. 4A), rendering no evidence for metamorphic devolatilization of ^{15}N-depleted

445   nitrogen from organics. $\delta^{15}N_{bulk}$ and % total nitrogen (TN) show only a loose positive

446   correlation (with $R^2 = 0.34$; Extended Data Fig. 5A), in the opposite direction of what would

447   be expected from significant loss of ^{15}N-depleted N from whole rocks via devolatilization.

448   Only a weak negative correlation exists between wt % TOC and $\delta^{13}C_{org}$ ($R^2 = 0.42$; Extended

449   Data Fig. 4C), also inconsistent with significant devolatilization of ^{13}C-depleted carbon

450   during metamorphism. These data indicate that loss of N during metamorphism and deep

451   burial did not significantly alter the primary $\delta^{15}N$ (or $\delta^{13}C$) values.

452   Nitrogen isotope exchange can occur between rocks and N-containing compounds

453   when fluids migrate during organic matter maturation[39]. Similar to metamorphism, offset

454   during thermal maturation generally results from preferential volatilization of ^{15}N-depleted

455   nitrogen from organic molecules. The $\delta^{15}N$ of the natural gas is highly variable, but can have

456    $\delta^{15}N$ as low as -12‰[40,41]. Nitrogen isotope exchange during fluid migration would tend to

457   homogenize the isotopic composition of participating N pools, decreasing the isotopic range

458   within the organic N pool and differences between organic and inorganic N pools[39]. Bulk-

459   rock $\delta^{15}N$ ($\delta^{15}N_{bulk}$) covers the measured range of $\delta^{15}N_{org}$, but are generally more positive

460   than $\delta^{15}N_{org}$, inconsistent with complete isotopic homogenization.

461   We observe only a very weak negative correlation between $\delta^{15}N_{bulk}$ and TOC:TN (R^2

462    $= 0.29$; Extended Data Fig. 5B), suggesting that some ^{15}N-enriched ammonium could have

463   been sorbed onto and/or incorporated into clay minerals in very low-TOC sediments,

464   presumably during exchange with post-depositional fluids. The % TN (but not $\delta^{15}N_{bulk}$)

465   indeed shows a significant positive correlation with % K_2O ($R^2 = 0.81$; Extended Data Fig.

466   5C), supporting incorporation of N into illites during K-metasomatism; however, there is no

467   correlation between $\delta^{15}N_{bulk}$ and % K_2O ($R^2 = 0.10$; Extended Data Fig. 5D), suggesting that

468   this exchange did not significantly affect bulk $\delta^{15}N$ values.

469

Data Availability Statement

470

471   All data generated or analysed during this study are included as source data in this

472 published article.

473

474 **Extended Data Legends**

475 Extended Data Figure 1. Results from statistical analysis of the $\delta^{15}N$ database, as detailed in

476 the Methods.

477

478 Extended Data Figure 2. Stratigraphic context for the Rooihoogte and Timeball Hill

479 formations within the Eastern Transvaal basin, South Africa, and associated ages. "MIF"

480 denotes the disappearance of the mass independent fractionation of sulfur isotopes in the

481 underlying Duitschland Formation (now known to reappear in the Rooihoogte Formation[6]).

482 Modified from Rasmussen *et al.*[5].

483

484 Extended Data Figure 3. Simplified geologic map of the Transvaal Supergroup outcrop area

485 (modified from Guo *et al.*[42]), showing the location of drill-core EBA-2. The core is currently

486 stored at the National Core Library at Donkerhoek, which is managed by the Council for

487 Geoscience in South Africa.

488

489 Extended Data Figure 4. Cross-plots of kerogen N abundance (% N_{org}) and $\delta^{15}N$ ($\delta^{15}N_{org}$, in

490 ‰), total organic carbon (% TOC) and organic $\delta^{13}C$ ($\delta^{13}C_{org}$, in ‰). For all datapoints, errors

491 are within the size of the symbols.

492

493   Extended Data Figure 5. Cross-plots of bulk-rock data, including A. bulk-rock δ^{15}N (δ^{15}N$_{bulk}$,

494   in ‰) versus total nitrogen (% TN), B. δ^{15}N$_{bulk}$ versus TOC:TN atomic ratios, C. % TN

495   versus K$_2$O content (%), and D. δ^{15}N$_{bulk}$ versus K$_2$O content. For all datapoints, errors are

496   within the size of the symbols.
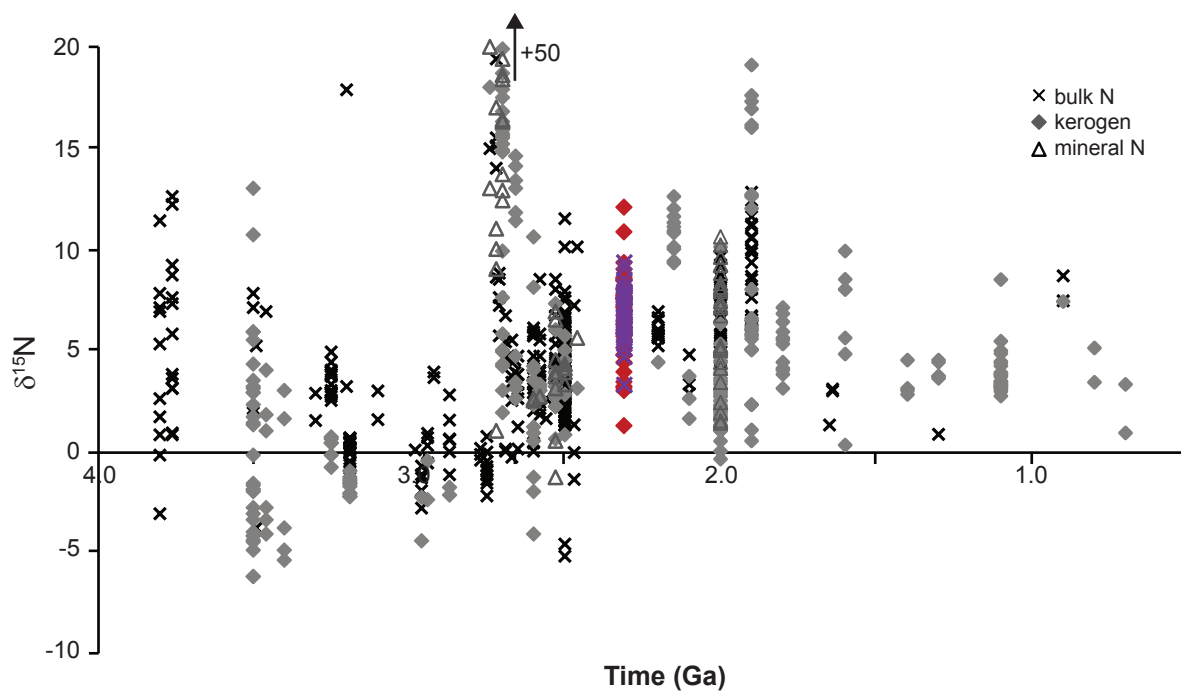
497

498   **Additional References**

499   30   Thomazo, C. & Papineau, D. Biogeochemical cycling of nitrogen on the early Earth.

500   *Elements* **9**, 345-351 (2013).

501   31   Stueken, E. E., Buick, R. & Schauer, A. J. Nitrogen isotope evidence for alkaline

502   lakes on late Archean continents. *Earth and Planetary Science Letters* **411**, 1-10

503   (2015).

504   32   McKirdy, D. M. & Powell, T. G. Metamorphic alteration of carbon isotopic

505   composition in ancient sedimentary organic matter: New evidence from Australia.

506   *Geology* **2**, 591-595 (1974).

507   33   Coplen, T. B. *et al.* New guidelines for delta C-13 measurements. *Analytical*

508   *Chemistry* **78**, 2439-2441, doi:10.1021/ac052027c (2006).

509   34   Polissar, P. J., Fulton, J. M., Junium, C. K., Turich, C. H. & Freeman, K. H.

510   Measurement of 13C and 15N isotopic composition on nanomolar quantitites of C and

511   N. *Analytical Chemistry* **81**, 755-763 (2009).

512   35   Boyd, S. R. & Philippot, P. Precambrian ammonium biogeochemistry: a study of the

513   Moine metasediments, Scotland. *Chemical Geology* **144**, 257-268 (1998).

514   36   Robinson, R. S. *et al.* A review of nitrogen isotopic alteration in marine sediments.

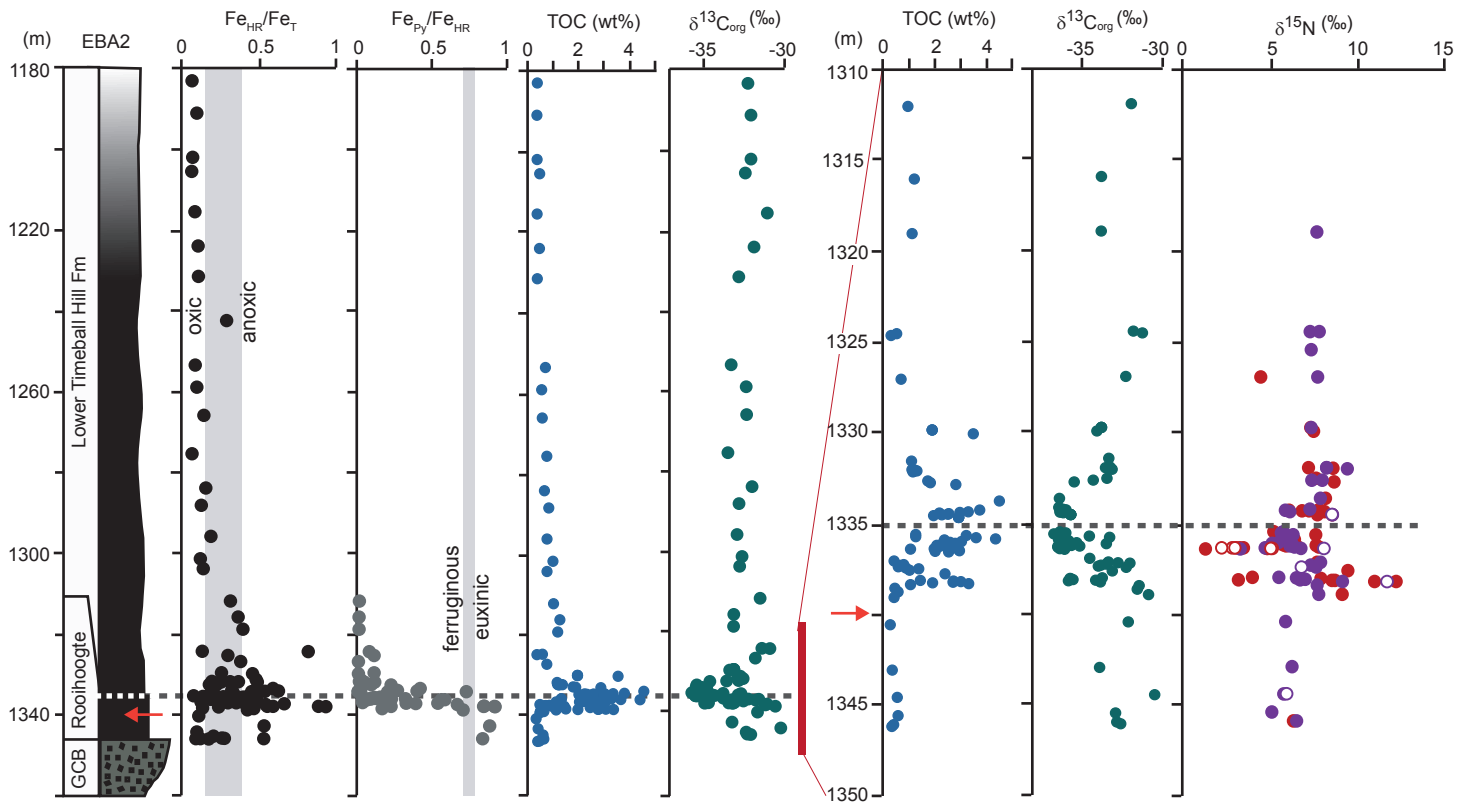515   *Paleoceanography* **27**, doi:10.1029/2012pa002321 (2012).

516   37   Bebout, G. E. & Fogel, M. L. Nitrogen-isotope compositions of metasedimentary

517   rocks in the Catalina Schist, California: Implications for metamorphic devolatilization

518   history. *Geochimica et Cosmochimica Acta* **56**, 2839-2849 (1992).

519   38   Ader, M., Boudou, J.-P., Javoy, M., Goffe, B. & Daniels, E. Isotope study of organic

520   ntrogen of Westphalian anthracites from the Western Middle field of Pennsylvania

521   (U.S.A.) and from the Bramsche Massif (Germany). *Organic Geochemistry* **29**, 315-

522   323 (1998).

523   39   Schimmelmann, A. & Lis, G. P. Nitrogen isotopic exchange during maturation of

524   organic matter. *Organic Geochemistry* **41**, 63-70,

525   doi:10.1016/j.orggeochem.2009.01.005 (2010).

526   40   Hoering, T. C. & Moore, H. E. The isotopic compositions of the nitrogen in natural

527   gases and associated crude oils. *Geochimica et Cosmochimica Acta* **13**, 225-232,

528   doi:10.1016/0016-7037(58)90024-3 (1958).

529   41   Murty, S. V. S. Noble-gases and nitrogen in natural gases from Gujarat, India.

530   *Chemical Geology* **94**, 229-240, doi:10.1016/0168-9622(92)90015-3 (1992).

531   42   Guo, Q. J. *et al.* Reconstructing Earth's surface oxidation across the Archean-

532   Proterozoic transition. *Geology* **37**, 399-402, doi:10.1130/g25423a.1 (2009).

533

534

535

KEY: chert breccia   black shale to siltstone